Artículo en edición

Tropical-Subtropical South American midsummer precipitation under ENSO events

Santiago I. Hurtado[1,2,3,*] , Eduardo A. Agosta[2,3] , Pablo G. Zaninelli[2,3,4]

[1]Instituto de Investigaciones Forestales y Agropecuarias Bariloche (IFAB), INTA-CONICET, San Carlos de Bariloche, Río Negro, Argentina

[2]Facultad de Ciencias Astronómicas y Geofísicas de la Universidad Nacional de La Plata (UNLP-FCAG), La Plata, Buenos Aires, Argentina

[3]Consejo Nacional de Investigaciones Científicas y Técnicas (CONICET), Buenos Aires, Argentina

[4] Instituto de Geociencias (IGEO), Consejo Superior de Investigaciones Científicas (CSIC)-Universidad Complutense de Madrid, Madrid, España UMI3351-IFAECI/CNRS-CONICET-UBA

***Corresponding author:** santiagoh719@gmail.com

Manuscrito recibido el 6 de febrero de 2023, en su versión final el 12 de junio de 2023

Abstract

El Niño-Southern Oscillation (ENSO) is the major forcing of interannual precipitation variability over South America (SA), especially from September to December, through a convection dipole over the South Atlantic Convergence Zone (SACZ) region and southeastern SA (SESA). However, the forcing mechanisms for midsummer (January) precipitation under ENSO events is less known. A cluster analysis applied to January OLR anomalies over Tropical-Subtropical SA under ENSO events depicts two clusters linked to the signs of the convection dipole between SACZ region and SESA. Most La Niña (LN) events (10 out of 13 events) are associated with enhanced convection over SESA and inhibited convection over SACZ region in January. El Niño (EN) events show both signs of the convection dipole in equal proportions, evidencing a non-linear response. In January, for EN and LN, enhanced (inhibited) convection over SESA and inhibited (enhanced) convection over SACZ region are associated with anticyclonic (cyclonic) tropospheric circulation over southeast Brazil, as observed in EN (LN) spring. During LN events, lower tropospheric circulation in January depends on the local thermodynamic conditions over central east Brazil in the previous months (Nov-Dec). If there are dry and warm (wet and cold) conditions over central east Brazil in Nov-

Dec, a thermal low (high) sets up. In contrast, under EN events if the dry and warm conditions over east Brazil in Nov-Dec are overall weak, an anticyclonic tropospheric circulation is established in southeast Brazil in January due to a predominant large-scale anomalous Walker cell. Lastly, the studied relationship may be used to build and assess sub-seasonal forecasting tools for January precipitation anomalies.

Keywords: ENSO, Teleconnection, midsummer precipitation, SESA, SACZ

Precipitación de verano en Sudamérica tropical-subtropical bajo eventos ENOS

El Niño-Oscilación del Sur (ENOS) es el principal forzante de la variabilidad de la precipitación interanual sobre Sudamérica (SA), especialmente de septiembre a diciembre, a través de un dipolo de convección sobre la región de la Zona de Convergencia del Atlántico Sur (SACZ) y sobre el sureste de SA (SESA). Los mecanismos forzantes de la precipitación de enero bajo eventos ENOS están menos conocidos. Un análisis de grupos aplicado a las anomalías OLR de enero sobre SA Tropical-Subtropical bajo eventos ENOS muestra dos grupos vinculados a los dos signos del dipolo de convección entre la región de la SACZ y SESA. La mayoría de los eventos La Niña (LN, 10 de 13 eventos) están asociados con una convección aumentada sobre SESA e inhibida sobre la región de la SACZ en enero. Los eventos El Niño (EN) muestran ambos signos del dipolo de convección en proporciones iguales, evidenciando una respuesta no lineal. En enero, para EN y LN, la convección aumentada (inhibida) sobre SESA y la convección inhibida (aumentada) sobre la región SACZ están asociadas con la circulación troposférica anticiclónica (ciclónica) sobre el sureste de Brasil, como se observó en la primavera para EN (LN). Durante los eventos LN, la circulación troposférica en niveles bajos en enero depende de las condiciones termodinámicas locales sobre el centro este de Brasil en los meses anteriores (noviembre-diciembre). Si hay condiciones secas y cálidas (húmedas y frías) sobre el centro este de Brasil en noviembre-diciembre, se establece una baja (alta) térmica. Por el contrario, bajo eventos EN, si las condiciones secas y cálidas sobre el este de Brasil en noviembre-diciembre son débiles en general, se establece una circulación troposférica anticiclónica en el sureste de Brasil en enero debido a una celda de Walker anómala predominante en gran escala. Por último, la relación estudiada puede usarse para construir y evaluar herramientas de pronóstico subestacional de las anomalías de precipitación de enero.

Palabras Claves: ENOS, Teleconecciones, precipitación de verano, SESA, SACZ

1. Introduction

The leading mode of summer precipitation variability over South America (SA) is a convection dipole in the tropic-subtropic between the South Atlantic Convergence Zone (SACZ; Van Der Wiel et al, 2015) region and southeastern SA (SESA), identified by the outgoing long-wave radiation (OLR) fields (Junquas et al, 2012; Vera et al, 2006). One sign of the dipole is associated with anticyclonic tropospheric circulation in lower levels that enhances moisture convergence in SESA through a strengthening of the moisture flux (MF) from the tropics and inhibits convection in the SACZ region by imposing stronger trades (Hurtado et al. 2023, Ma et al, 2011). While the other sign of the dipole is associated with cyclonic tropospheric circulation in lower levels that fosters the opposite anomalous conditions (Hurtado et al. 2023, Ma et al, 2011; Vera et al, 2006). Its time-scale ranges from sub-monthly to interannual in association with different drivers such as: changes in the South American Low-Level Jet (SALLJ; e.g. Montini et al, 2019), sub-monthly Rossby wave trains (e.g. Van Der Wiel et al, 2015), the Madden-Julian Oscillation (MJO; e.g. Alvarez et al, 2016), and the El Niño-Southern Oscillation (e.g. ENSO; Hurtado and Agosta, 2021).

The ENSO is by far the major forcing of SA precipitation at interannual time-scales (Grimm, 2011). There is a high consensus that in austral spring and early summer (September–December) the ENSO modulates SA precipitation through an upper-level extratropical Rossby wave train across the South Pacific that imposes the low-level circulation anomalies linked to the SA precipitation dipole (Cai et al, 2020; Cazes-Boezio et al, 2003; Grimm, 2003; Grimm and Zilli, 2009; Hurtado and Agosta, 2021; Tedeschi et al, 2015, among others). In this sense, El Niño (EN) events are associated with enhanced convection in SESA and inhibited convection in the SACZ region, while La Niña (LN) events are associated with the inverse situation (Hurtado and Agosta, 2021). In midsummer (January), instead, consensus on the precipitation modulation by ENSO is less strong. On one hand, according to Grimm et al (2007) the precipitation signal in January is reversed compared to the signal in spring. By means of numerical simulations, the authors proposed an explanatory mechanism through the generation of localized thermal pressure low/high over southeastern Brazil, owing to local thermo-

dynamic process in late spring-early summer. On the other hand, Cazes-Boezio et al (2003) and Hurtado and Agosta (2021) found from observations that the ENSO spring signal is maintained from September to January, though the forcing mechanism for January precipitation is not discernible.

In consequence, because of the discrepancy between results and the explanatory mechanism found for ENSO modulation over precipitation in midsummer, the present work aims at determining the physical mechanisms leading to the observed January precipitation anomalies over tropical-subtropical SA during ENSO events.

2. Data and methods

The NOAA observed-interpolated OLR data provided by the NOAA PSL, Boulder, Colorado, USA in the period 1979-2020 (retrieved from their website https://psl.noaa.gov/), were used as a proxy of precipitation anomalies in tropical-subtropical SA. It consists of a gridded data-set with temporal integration on a regular grid of 2.5° latitude × 2.5° longitude (Liebmann and Smith, 1996). The study domain was tropical-subtropical SA defined (for this study) from 5°S to 36° S and from 70°W to 30°W. To compare the OLR data with precipitation data, the CRU TS4.05 precipitation climate dataset, with a 0.5-degree spatial resolution was used (Harris et al., 2020).

The nino12, nino3, nino34, and nino4 indexes were used to evaluate ENSO conditions, retrieved from https://www.psl.noaa.gov/data/climateindices/list/. Particularly, nino34 index was used to define EN and LN events, following the conventional definition (see the EN and LN events in Table 1). For a description of the conventional definitions of ENSO events see: https://origin.cpc.ncep.noaa.gov/products/analysis_monitoring/ensostuff/ONI_v5.php. To assess potential relationships with different climate drivers, other climate indexes were used: the Indian Ocean Dipole Index (IOD, (Saji y Yamagata, 2003)) retrieved from http://www.bom.gov.au/, and the Southern Annular Mode Index (SAM, Marshall 2003) retrieved from http://www.nerc-bas.ac.uk/icd/gjma/sam.html.

To identify common groups of midsummer precipitation under ENSO events, a k-means cluster analysis was performed using the January OLR data for the ENSO years (see Table 1). First, a

principal component analysis (PCA) was applied to the OLR anomalies over the domain of tropical-subtropical SA to reduce the dimension of the problem (Wilks, 2011). Then, the first 12 principal components were used in the clustering procedure, since they retain 90% of the variability. The k-means algorithm needs to set the amount of clusters (k). For doing so, the k-means algorithm was run 1.000 times for each k (up to 5 clusters) with different random seeds and then for each k the defined clusters are the ones with the lowest Within-Cluster-Sum-of-Squared-Errors. Then, k is determined using the Silhouette coefficient since it measures both the cohesion and separation of clusters (Dinh et al, 2019). Cohesion is a measure of how similar the data of the same cluster are, while separation measures how different the data between clusters are.

Atmospheric variables on a 0.25° latitude-longitude grid from the ECMWF ERA5 reanalysis were used (Hersbach et al, 2019a,b, 2020). The dataset covers the 1979–2020 period. The used reanalysis data consist in: geopotential height (GH) and wind at 250hPa and 850hPa, omega (ω) and wind divergence in all vertical levels, Mean Sea Level Pressure (MSLP), Skin Temperature (SkT), and the vertically integrated MF (VIMF) and its divergence. Furthermore, some derived variables were calculated: the potential velocity (CHI) and the wave activity flux (Wflux; Takaya and Nakamura, 2001) at 250hPa, and the stream-function at 850 hPa.

To test relationships between Cluster numbers under EN or LN with high and low values of climate indices (SAM and IOD), contingency tables were built and tested with the chi-squared test (Wilks, 2011). The null hypothesis of the chi-squared test is that the data is independent.

To explore the physical mechanisms, composites of different climate variables were done. The anomalies of the composites were tested using the two-tailed unequal-variance Student's t-test at a significance level α=.10 (Moser and Stevens, 1992; Wilks, 2011). Variable anomalies are estimated in the 1980-2010 baseline without de-trending. It was tested if they are sensitive to baseline changes along the period 1979-2020 due to trends, by comparing anomalous fields obtained with two different baselines, 1980-2000 and 2000-2020. The anomaly differences between baselines are insignificant over the domain. Therefore anomalies are not sensitive to changes in the baseline. This implies that trend-induced anomalies throughout the period 1979-2020 are not relevant over the domain and do not compromise the analysis. All graphics and computations were done using R, in particularly six packages were used: ClusterR

(Mouselimis, 2022), dplyr (Wickham et al, 2022), ggplot2 (Wickham, 2016), ggforce (Pedersen, 2020), ggh4x (van den Brand, 2020) and metR (Campitelli, 2020).

3. Results

3.1 Clusters

A cluster analysis of OLR anomalies for January under ENSO events was done to identify groups of common OLR patterns. This was done in order to further examine their forcing mechanism. The Silhouette coefficient yielded the highest value for two clusters, and so this amount was used. In this sense, all January's under ENSO events (see Table 1) were classified into two clusters regarding their OLR anomaly (see Table 2). To show the characteristics of each cluster, the anomalous OLR and precipitation composite for each cluster are shown in Figure 1. Cluster 1 presents enhanced convection over SESA region and inhibited convection over SACZ region. Whereas, Cluster 2 presents the opposite sign anomalous dipole. In this sense, Cluster 1 (2) OLR composite resembles the linkage between EN (LN) events with the precipitation dipole in spring (Cai et al, 2020; Cazes-Boezio et al, 2003; Hurtado and Agosta, 2021; among others).

Table 2 shows the ENSO events in January, classified for each OLR cluster. On one hand, the EN events in January are evenly distributed, half of them in Cluster 1 and the other half in Cluster 2. On the other hand, the LN events in January are mostly classified into Cluster 1 (10 out of 13). This depicts a non-linear relationship between the convection dipole and ENSO events in January. In the following sections, the forcing mechanisms for these groups will be analyzed.

3.2 Regional circulation

To assess the drivers of each cluster, first, the regional circulation is analyzed. The EN events in cluster 1 are characterized by enhanced convection over SESA and inhibited convection over SACZ (Fig. 2 panels a1). Whereas EN events in cluster 2 present the opposite sign dipole but with lower anomalies over SESA (Fig. 2 panels a2). This OLR dipole seems to be generated by positive (negative) low-level stream-function anomalies in southeast Brazil that lead to an

enhancement (inhibition) VIMF from the tropics to SESA (Fig. 2 panels b1 and b2). The regional anomalous circulation fosters VIMF divergence and omega anomalies at 500hPa (not shown) in SESA and SACZ regions that generate the observed OLR dipole (Fig. 2 panels a1 - a2). The LN events in clusters 1 and 2 present an OLR dipole like the one observed for the EN events in clusters 1 and 2, respectively, but with lower intensities (Fig. 3 panels a1-a2). As for the EN events, the OLR dipole in the LN events is associated with an anomalous anticyclonic circulation for cluster 1 and with an anomalous cyclonic circulation for cluster 2 (Fig. 3 panels b1-b2). The low significance of the anomalies for the LN events in cluster 2 is due to the small sample size of the composite. This configuration of a cyclonic/anticyclonic circulation over southeastern Brazil that fosters a convection dipole is a common feature in austral summer (Hurtado et al. 2023).

3.3 Previous months' conditions

Grimm et al. (2007) showed through numerical simulations that dry and hot (wet and cold) conditions in central-eastern Brazil in the months prior to January, sets up a thermal low (high) in January due to local processes. Through this mechanism Grimm et al. (2007) explained the reversal of precipitation anomalies found by Grimm (2003) for EN events, and by Grimm (2004) for LN events. Considering this mechanism, the thermodynamic conditions of the bimester November-December prior to the analyzed Januaries are further explored in Figure 4. For both EN groups, enhanced VIMF is observed from the tropics to the subtropics, evidencing an intensification of the SALLJ, and, in consequence, enhanced convection is observed in SESA (Fig. 4 panels a1-a2 and b1-b2). Positive OLR anomalies are higher and significant areas are wider over Brazil for the EN events in cluster 2 compared to the ones in cluster 1, meaning more inhibited convection in the former (Fig. 4 panels a1-a2). As expected, these positive OLR anomalies are accompanied by warmer SkT anomalies (Fig. 4 panels c1-c2). So, EN events in Clusters 1 and 2 present dry and hot conditions in the previous months being greater in Cluster 2. According to the mechanism proposed by Grimm et al. (2007), these conditions would set up a thermal low in January but such a system is observed only for EN events in Cluster 2 (see Figure 2 panel b2). This may imply that for EN events in Cluster 1, the thermal low did not set up since their dry and hot anomalies in previous months are weaker or that another process prevails.

The LN events in cluster 1 show tropospheric circulation features as opposed to the EN events in cluster 2. Thus, LN events in cluster 1 present VIMF anomalies, evidencing a weakening of the SALLJ, that propitiate an OLR dipole with enhanced convection over SACZ region and inhibited convection over SESA (Fig. 4 panels a3 and b3). The anomalous wet and cloudy conditions over Brazil are associated with negative SkT anomalies (Fig. 4 panels c3). In contrast, LN events in cluster 2 tend to show dry and warm anomalies over Brazil (Fig. 4 panels a-c4) as those observed in EN events in cluster 2 though with lower amplitudes. Considering Grimm et al (2007) mechanism, the regional circulation observed in January under LN events (Fig. 3 panels b1-b2) is consistent with the previous month's thermodynamic conditions.

Putting all together, the results from Figure 4 together with Figures 2 and 3 indicate that Grimm et al (2007) mechanism may explain precipitation in January over SA during LN events and for EN events in Cluster 2. But can not account for the observed anomalies of EN events in Cluster 1. Therefore, in the next section, the drivers of EN events in Cluster 1 are assessed.

3.4 Remote teleconnections for EN events in Cluster 1

The GH anomalies and the Wflux in upper levels are overall weak and there is not a marked structure of a Rossby wave train that predominates (Fig. S1). In the absence of Rossby wave trains in upper levels (Fig. S1), the negative stream-function composite anomalies in southeastern Brazil, observed in the EN events in cluster 1, appear to be due to an anomalous Walker cell (Fig. 5). The anomalous Walker-cell circulation is a typical feature of EN events (Cai et al, 2020). This is evidenced by the MSLP and CHI at 250hPa composite anomaly fields that present a zonal asymmetry in the tropics with positive anomalies over Brazil and the Atlantic Ocean and negative anomalies over the Pacific Ocean (Fig. 5 panels a and b). An anomalous 3-D configuration of the Walker cell is further confirmed by the omega and divergence composite anomaly field that shows upward anomalous motion in the central Pacific and downward anomalous motion over Brazil and the tropical Atlantic (Fig. 5 panel c). The downward branch of the Walker-cell imposes the observed anticyclonic circulation over Brazil (Fig. 2 panel b1).

It seems that the convection dipole in January during EN events depends on the intensity of dry and warm conditions in central-east Brazil during the previous spring months. If dry and warm conditions in Nov-Dec are overall weak (Fig 4 panels a1-b1-c1), an anticyclonic circulation is established in January (Fig. 2 b1) due to a predominant large-scale anomalous Walker cell (Fig. 5). On the contrary, if dry and warm conditions are overall intense (Fig 4 panels a2-b2-c2), a localized thermal cyclonic circulation sets up (Fig. 2 b2), as was proposed by Grimm et al (2007).

3.5 Relationship with climate drivers

It is known that ENSO phenomena interact with other climate drivers such as the IOD (Reboita et al., 2021) or SAM (Vera and Osman, 2018). Owing to this, in this section, we explore if there is any dependence on the Clusters with respect to IOD and SAM index. For doing so, we define "SAM+" events as those whose SAM index is over its percentile 75, "SAM-" as those with lower values than the percentile 25, and "SAM Neu" as those between percentile 25 and 75. In the same way, "IOD+", "IOD-", and "IOD Neu" events were defined. Figure 6 shows the contingency tables for all groups (EN and LN in Clusters 1 and 2) and all SAM and IOD categories. A great dispersion is observed with no clear differentiation between EN Cluster 1 and EN Cluster 2. The same appears to happen between LN Cluster 1 and LN Cluster 2. In order to objectively test these appreciations, the contingency tables (EN~IOD, EN~SAM, LN ~ IOD, and LN~SAM) were tested with the chi-squared test (Wilks, 2011). For all cases the p-value of the test was greater than 0.1, so the null hypothesis can not be rejected, implying a non-dependence of the Clusters with SAM or IOD.

Given that no apparent distinctive association was found between EN and LN clusters with other climate drivers, the amplitude difference between ENSO indices were explored. The nino1.2, nino3, nino3.4 and nino4 ENSO indices from November to February are shown in Fig 7, discriminated in the ENSO phases (EN and LN) and Cluster number. It can be observed that there is a great dispersion of index values (SST anomalies) for each Cluster and ENSO phase. For the same ENSO phase, the mean value (stroked lines) of each index is almost equal between clusters. This is indicative that the differences found among ENSO Clusters do not depend on the magnitude of the ENSO-related SST anomalies.

4. Conclusions

This research focuses on the forcing mechanisms of midsummer precipitation over Tropical-Subtropical SA under ENSO events in the period 1979-2020. A cluster analysis on OLR anomalies yielded two groups for January under ENSO events that resemble the well-known SA convection dipole. OLR anomaly cluster 1 depicts a dipole with enhanced convection over SESA and inhibited convection over SACZ region, while OLR anomaly cluster 2 shows the opposite sign of the OLR dipole. 10 out of 13 LN events fall into Cluster 1, whereas 7 out of 14 EN events fall into Cluster 1, and the other 7 fall into Cluster 2. The latter paired frequencies evidence a non-linear response for EN events.

LN events in both clusters and EN events in cluster 2 are associated with a thermodynamic forcing that was established in previous months, in concordance with Grimm et al (2007). If there are dry and warm (wet and cold) conditions over central east Brazil in Nov-Dec, a localized thermal cyclonic (anticyclonic) tropospheric circulation sets up in January propitiating the OLR anomalies observed in cluster 2 (1). In contrast, the former lower level thermal cyclonic circulation is not established in January during EN events for cluster 1 in which dry and hot conditions in the previous month (Nov-Dec) are overall weak. EN events in cluster 1 are associated with a remote forcing through an anomalous Walker cell circulation in January, with rising motion in the central equatorial Pacific and sinking motion over eastern Brazil. Moreover, the differences between clusters do not appear to respond to differences in ENSO indices or other climate drivers such as SAM and IOD. So they may depend on internal atmospheric variability or lower-scale processes.

The current understanding of such a dependence on the thermodynamic conditions over central east Brazil in the months prior to January may contribute to improving seasonal precipitation forecasting over SESA and the SACZ region. In a nutshell, the relationship may be used to build and assess sub-seasonal forecasting tools for January precipitation anomalies in the studied regions based on monitoring precipitation and temperature conditions (i.e., via OLR satellite measures and/or monitoring weather station data) in central east Brazil. The present work establishes the physical bases for the design of such a forecasting tool, which could be developed in collaboration with the Climate Service of the National Weather Service to adequate it to potential users' applications. The latter is left for future research.

Acknowledgment

The current research was funded by the PPID-G008 from the National University of La Plata title: “Extremos húmedos y secos en Argentina. Análisis de los cambios proyectados para fines del siglo XXI.”. We wish to express our gratitude to the Carmelite NGO for the financial support.

References

Alvarez MS, Vera CS, Kiladis GN, Liebmann B (2016) Influence of the madden julian oscillation on precipitation and surface air temperature in south america. Climate Dynamics 46(1-2):245–262

Cai W, McPhaden MJ, Grimm AM, Rodrigues RR, Taschetto AS, Garreaud RD, Dewitte B, Poveda G, Ham YG, Santoso A, et al (2020) Climate impacts of the el niño–southern oscillation on south america. Nature Reviews Earth & Environment 1(4):215–231

Campitelli E (2020) metR: Tools for Easier Analysis of Meteorological Fields. DOI 10.5281/zenodo.2593516, URL https://github.com/eliocamp/metR , r package version 0.8.0

Cazes-Boezio G, Robertson AW, Mechoso CR (2003) Seasonal dependence of enso teleconnections over south america and relationships with precipitation in uruguay. Journal of Climate 16(8):1159–1176

Dinh DT, Fujinami T, Huynh VN (2019) Estimating the optimal number of clusters in categorical data clustering by silhouette coefficient. In: International Symposium on Knowledge and Systems Sciences, Springer, pp 1–17

Grimm AM (2003) The el niño impact on the summer monsoon in brazil: regional processes versus remote influences. Journal of Climate 16(2):263–280

Grimm, A. M. (2004). How do La Niña events disturb the summer monsoon system in Brazil?. Climate Dynamics, 22(2-3), 123-138.

Grimm AM (2011) Interannual climate variability in south america: impacts on seasonal precipitation, extreme events, and possible effects of climate change. Stochastic Environmental Research and Risk Assessment 25(4):537–554

Grimm AM, Zilli MT (2009) Interannual variability and seasonal evolution of summer monsoon rainfall in south america. Journal of Climate 22(9):2257–2275

Grimm AM, Pal JS, Giorgi F (2007) Connection between spring conditions and peak summer monsoon rainfall in south america: Role of soil moisture, surface temperature, and topography in eastern brazil. Journal of Climate 20(24):5929–5945

Harris, I., Osborn, T.J., Jones, P. et al. Version 4 of the CRU TS monthly high-resolution gridded multivariate climate dataset. Sci Data 7, 109 (2020). https://doi.org/10.1038/s41597-020-0453-3

Hersbach H, Bell B, Berrisford P, Biavati G, Horanyi A, Muñoz Sabater J, Nicolas J, Peubey C, Radu R, Rozum I, et al (2019a) Era5 monthly averaged data on pressure levels from 1979 to present. Copernicus Climate Change Service (C3S) Climate Data Store (CDS) 10

Hersbach H, Bell B, Berrisford P, Biavati G, Horanyi A, Muñnoz Sabater J, Nicolas J, Peubey C, Radu R, Rozum I, et al (2019b) Era5 monthly averaged data on single levels from 1979 to present. Copernicus Climate Change Service (C3S) Climate Data Store (CDS) 10

Hersbach H, Bell B, Berrisford P, Hirahara S, Horanyi A, Muñnoz-Sabater J, Nicolas J, Peubey C, Radu R, Schepers D, et al (2020) The era5 global reanalysis. Quarterly Journal of the Royal Meteorological Society

Hurtado SI, Agosta EA (2021) El niño southern oscillation-related precipitation anomaly variability over eastern subtropical south america: Atypical precipitation seasons. International Journal of Climatology.
https://doi.org/10.1002/joc.6559

Hurtado, S. I., Agosta, E. A., & Zaninelli, P. G. (2023). Monthly variations of forcing mechanisms of austral summer precipitation in subtropical Argentina. Atmospheric Research, 106609. https://doi.org/10.1016/j.atmosres.2023.106609

Junquas C, Vera C, Li L, Le Treut H (2012) Summer precipitation variability over southeastern south america in a global warming scenario. Climate dynamics 38(9):1867–1883

Liebmann B, Smith CA (1996) Description of a complete (interpolated) outgoing longwave radiation dataset. Bulletin of the American Meteorological Society 77(6):1275–1277

Ma HY, Ji X, Neelin J, Mechoso C (2011) Mechanisms for precipitation variability of the eastern brazil/sacz convective margin. Journal of climate 24(13):3445–3456

Marshall, G. J., 2003: Trends in the Southern Annular Mode from observations and reanalyses. J. Clim., **16,** 4134-4143, doi:10.1175/1520-0442%282003%29016<4134%3ATITSAM>2.0.CO%3B2

Montini TL, Jones C, Carvalho LM (2019) The south american low-level jet: a new climatology, variability, and changes. Journal of Geophysical Research: Atmospheres 124(3):1200–1218

Moser BK, Stevens GR (1992) Homogeneity of variance in the two-sample means test. The American Statistician 46(1):19–21

Mouselimis L (2022) ClusterR: Gaussian Mixture Models, K-Means, Mini-Batch-Kmeans, K-Medoids and Affinity Propagation Clustering. URL https://CRAN.R-project.org/package=ClusterR , r package version 1.2.6

Pedersen TL (2020) ggforce: Accelerating 'ggplot2'. URL https://CRAN.R-project.org/package=ggforce , r package version 0.3.2

Reboita, M. S., Ambrizzi, T., Crespo, N. M., Dutra, L. M. M., Ferreira, G. W. D. S., Rehbein, A., ... & Souza, C. A. D. (2021). Impacts of teleconnection patterns on South America climate. Annals of the New York Academy of Sciences, 1504(1), 116-153.

Saji, N. H., & Yamagata, T. J. C. R. (2003). Possible impacts of Indian Ocean dipole mode events on global climate. Climate Research, 25(2), 151-169.

Takaya K, Nakamura H (2001) A formulation of a phase-independent wave-activity flux for stationary and migratory quasigeostrophic eddies on a zonally varying basic flow. Journal of the Atmospheric Sciences 58(6):608–627

Tedeschi RG, Grimm AM, Cavalcanti IF (2015) Influence of central and east enso on extreme events of precipitation in south america during austral spring and summer. International Journal of Climatology 35(8):2045–2064

van den Brand T (2020) ggh4x: Hacks for 'ggplot2'. URL https://github.com/teunbrand/ggh4x , r package version 0.1.0.9000

Van Der Wiel K, Matthews AJ, Stevens DP, Joshi MM (2015) A dynamical framework for the origin of the diagonal south pacific and south atlantic convergence zones. Quarterly Journal of the Royal Meteorological Society 141(691):1997–2010

Vera, C. S., & Osman, M. (2018). Activity of the Southern Annular Mode during 2015–2016 El Niño event and its impact on Southern Hemisphere climate anomalies. International Journal of Climatology, 38, e1288-e1295.

Vera C, Higgins W, Amador J, Ambrizzi T, Garreaud R, Gochis D, Gutzler D, Lettenmaier D, Marengo J, Mechoso C, et al (2006) Toward a unified view of the american monsoon systems. Journal of climate 19(20):4977–5000

Wickham H (2016) ggplot2: elegant graphics for data analysis. springer

Wickham H, Francois R, Henry L, Muller K (2022) dplyr: A Grammar of Data Manipulation. URL https://CRAN.R-project.org/package=dplyr , r package version 1.0.9

Artículo en edición

Wilks DS (2011) Statistical methods in the atmospheric sciences, vol 100. Academic press

460

Table 1: El Niño and La Niña events in the period 1979-2020

462

El Niño	**La Niña**
1979/80, 1982/83, 1986/87, 1987/88, 1991/92, 1994/95, 1997/98, 2002/03, 2004/05, 2006/07, 2009/10, 2014/15, 2015/16, 2018/19	1983/84, 1984/85, 1988/89, 1995/96, 1998/99, 1999/00, 2000/01, 2005/06, 2007/08, 2008/09, 2010/11, 2011/12, 2017/18

Table 2: El Niño and La Niña events classified into each cluster.

Cluster 1		**Cluster 2**	
El Niño	**La Niña**	**El Niño**	**La Niña**
1986/87, 1987/88, 1994/95, 1997/98, 2009/10, 2014/15, 2018/19	1983/84, 1988/89, 1995/96, 1998/99, 1999/00, 2000/01, 2005/06, 2008/09, 2010/11, 2017/18	1979/80, 1982/83, 1991/92, 2002/03, 2004/05, 2006/07, 2015/16	1984/85, 2007/08, 2011/12

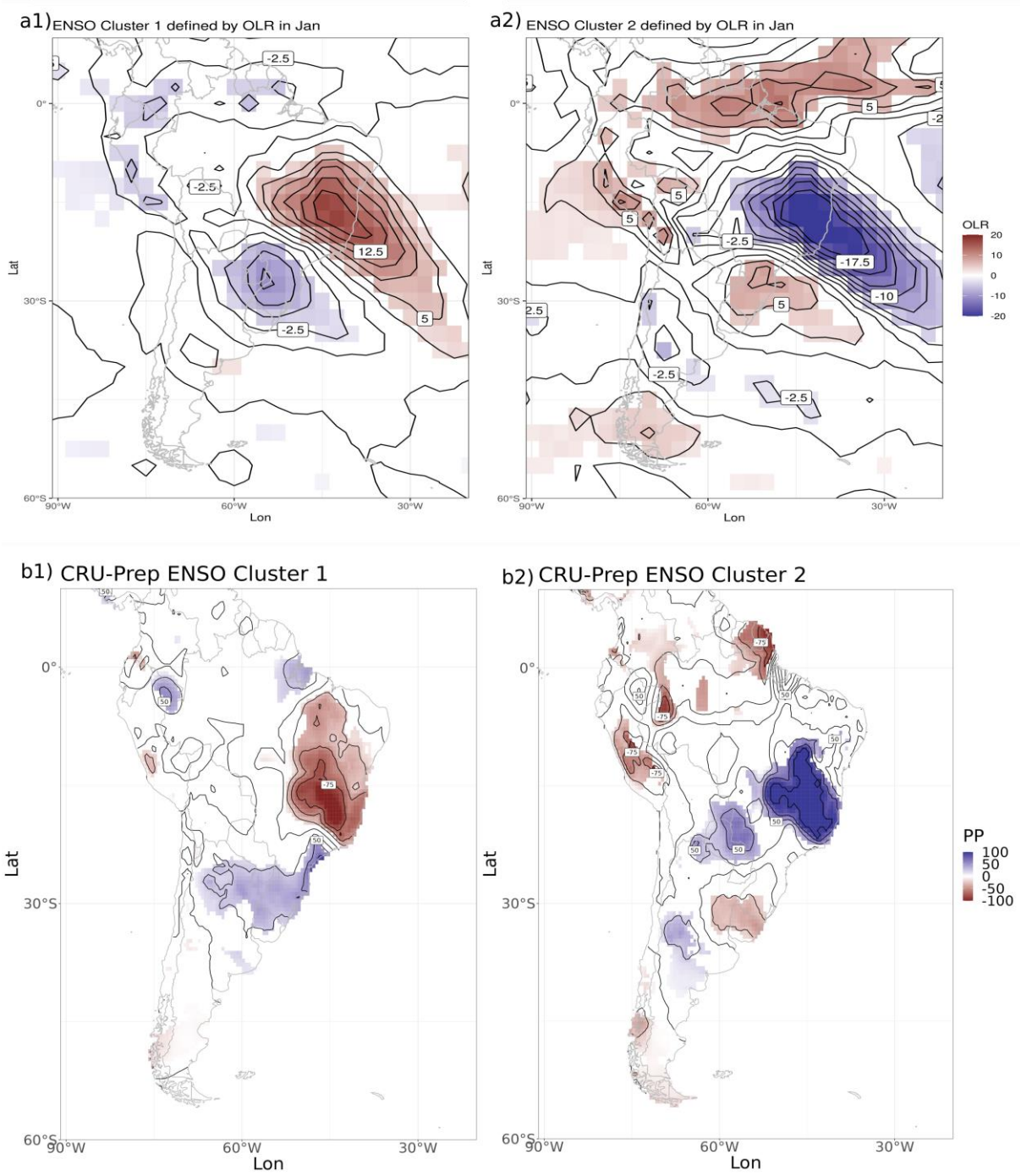

Figure 1. Composite OLR (panels a) and precipitation (panels b) anomaly fields of Cluster 1 (panels 1) and Cluster 2 (panels 2) in January. Color shades stand for significant anomalies at a 90% confidence level. The baseline period for the anomalies is 1980-2010.

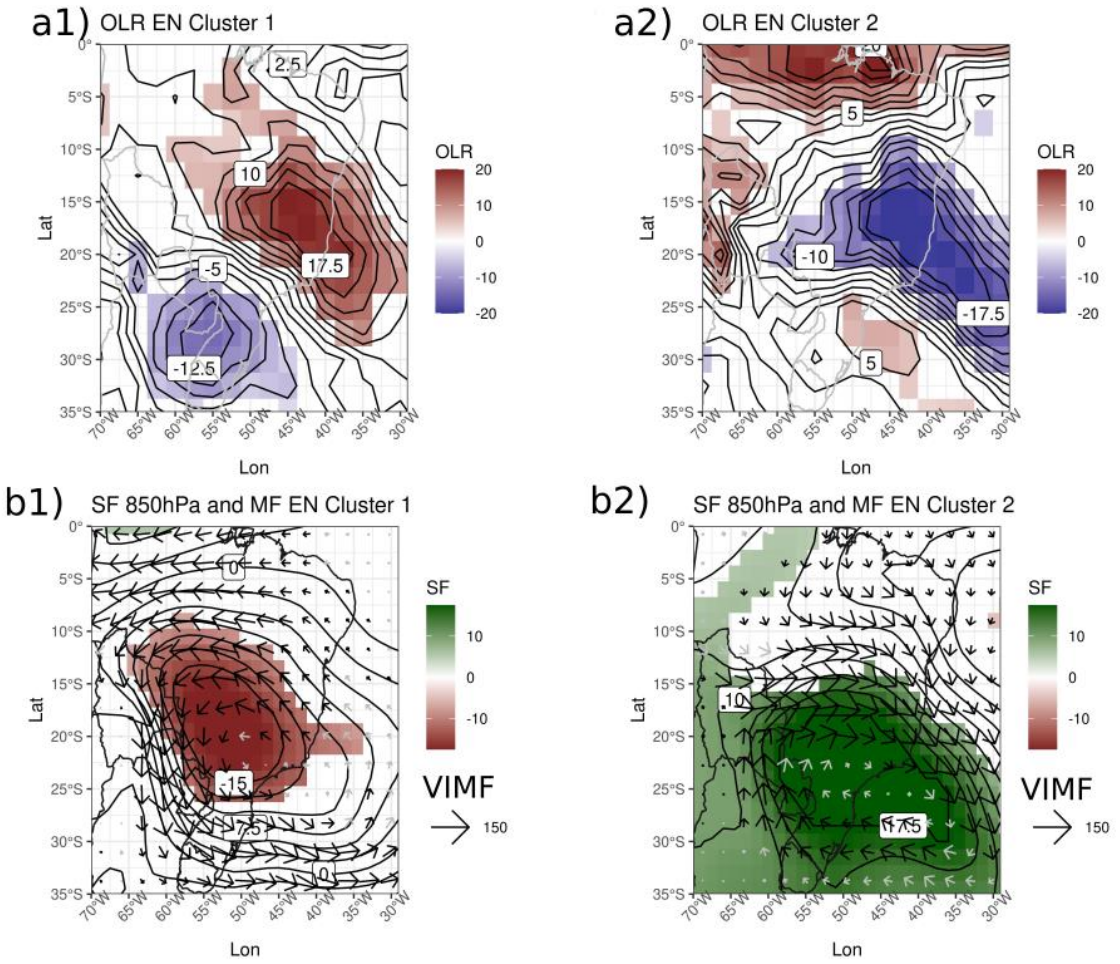

Figure 2. Upper panels: January OLR composite anomalies for the EN events in cluster 1 (panel a1) and for the EN events in cluster 2 group (panel a2). **Lower panels:** January stream-function at 850hPa (contours and color) and VIMF (arrows) composite anomalies for the EN events in cluster 1 group (panel b1) and for the EN events in cluster 2 group (panel b2). Color shades stand for significant anomalies at a 90% confidence level. Black arrows stand for significant VIMF anomalies at 90% confidence level. The baseline period for the anomalies is 1980-2010.

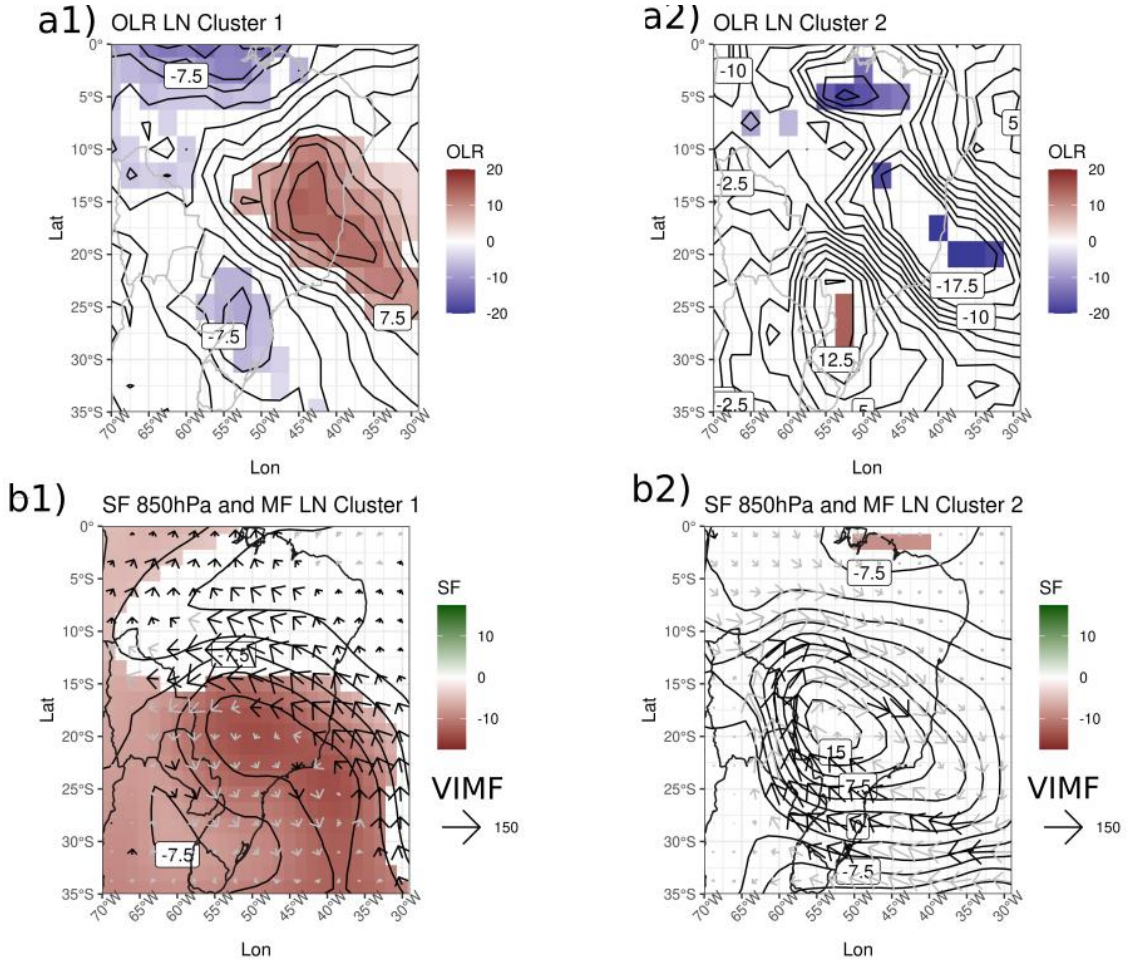

Figure 3. As Figure 2 but for LN events.

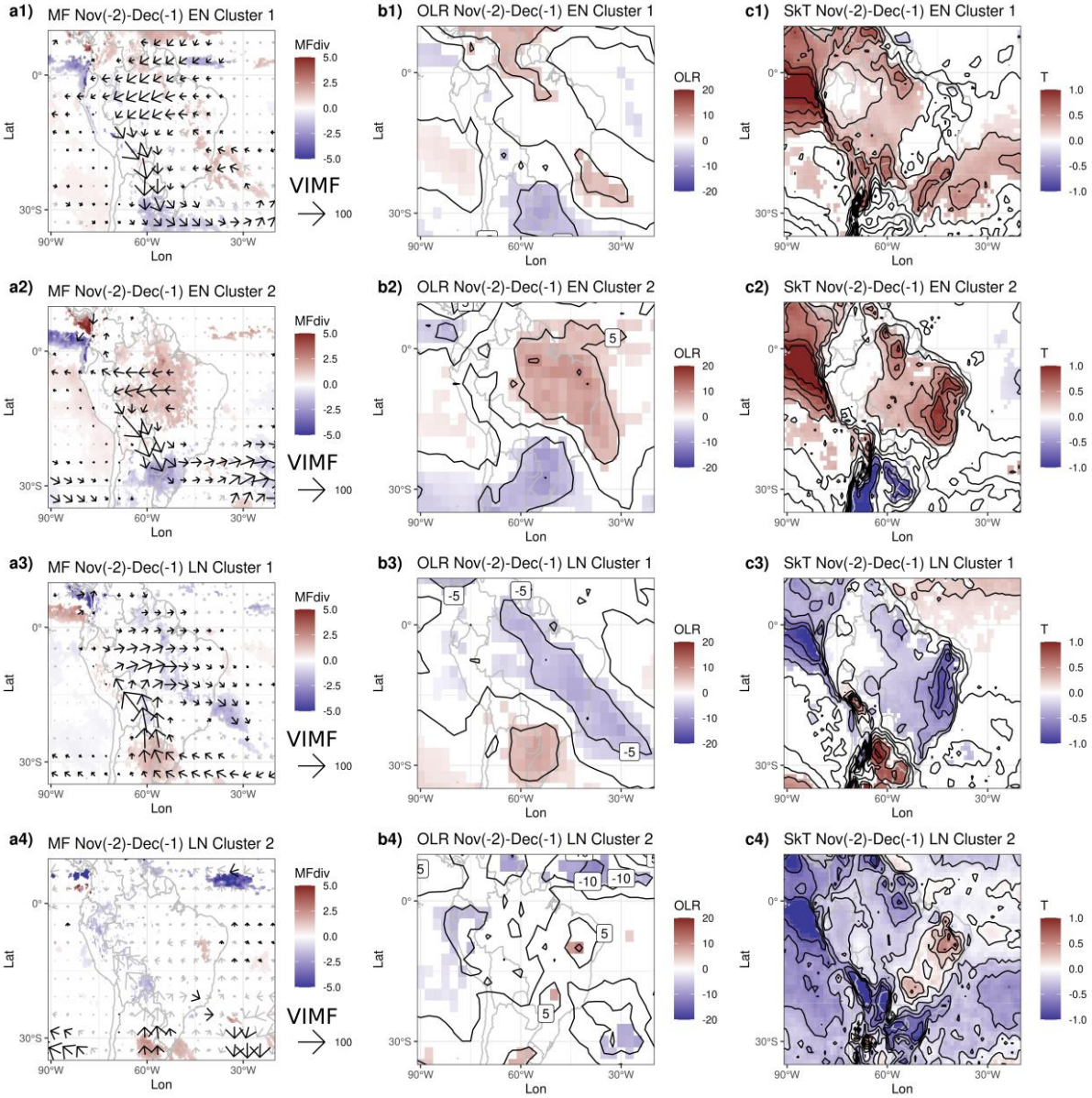

490 **Figure 4.** Composite anomalies of OLR (panels a), SkT (panels b), and VIMF and its divergence (panels c) for the two-month period November-December prior to January for the
492 EN events in cluster 1 group (panels 1), the EN events in cluster 2 group (panels 2), LN events in cluster 1 group (panels 3) and LN events in cluster 2 group (panels 4). Color shades stand
494 for significant anomalies at a 90% confidence level, except for panel c4 where all anomalies are colored regardless of whether they are statistically significant. Black arrows stand for
496 significant VIMF anomalies at 90% confidence level. The baseline period for the anomalies is 1980-2010.

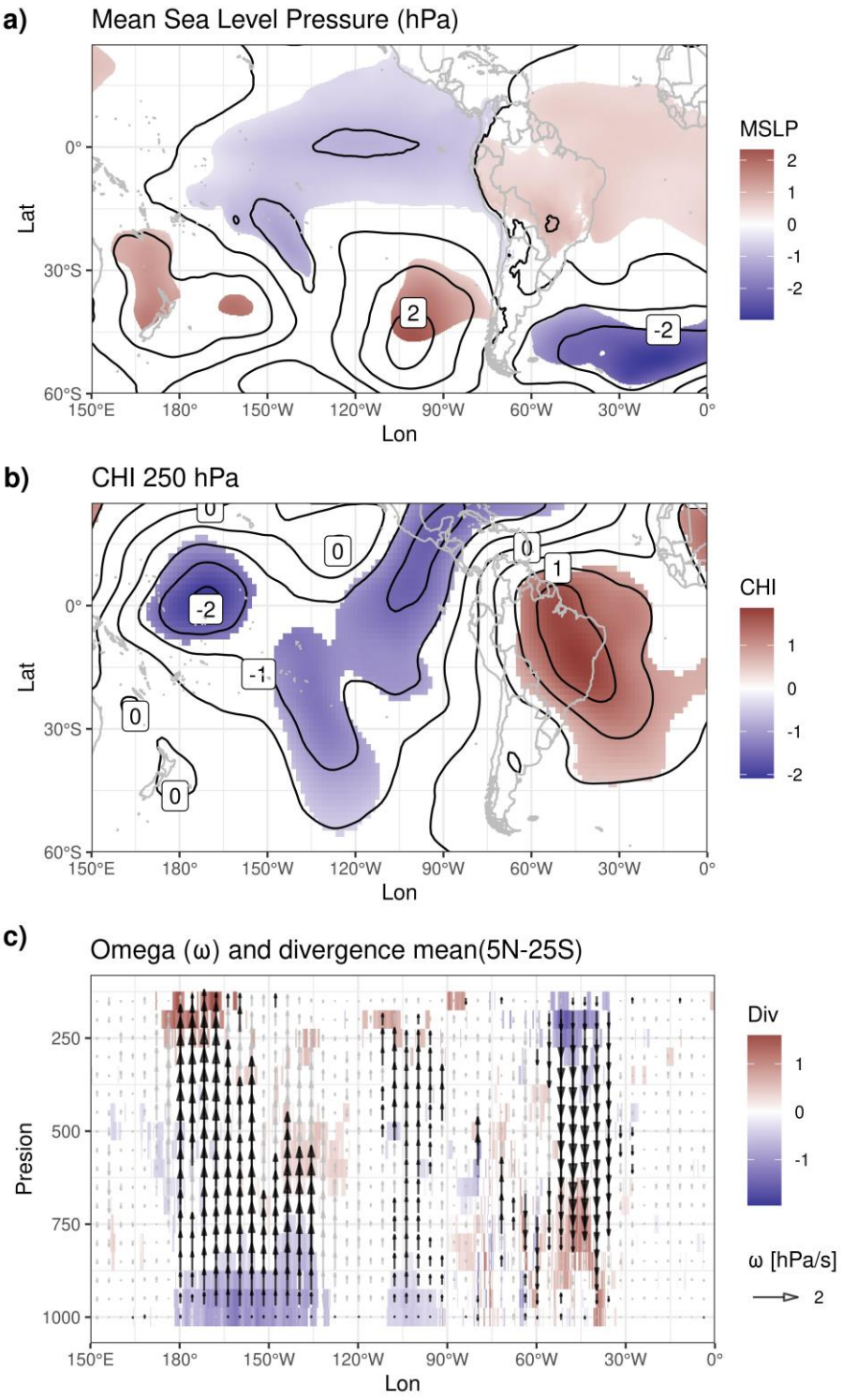

526 **Figure 5.** January MSLP composite anomalies (panel a), 250 hPa CHI anomalies (panel b),
and omega and wind divergence averaged between 5°N and 25°S (panel c) for the EN events
528 in cluster 1 group. Color shades stand for significant anomalies at a 90% confidence level. The
baseline period for the anomalies is 1980-2010.

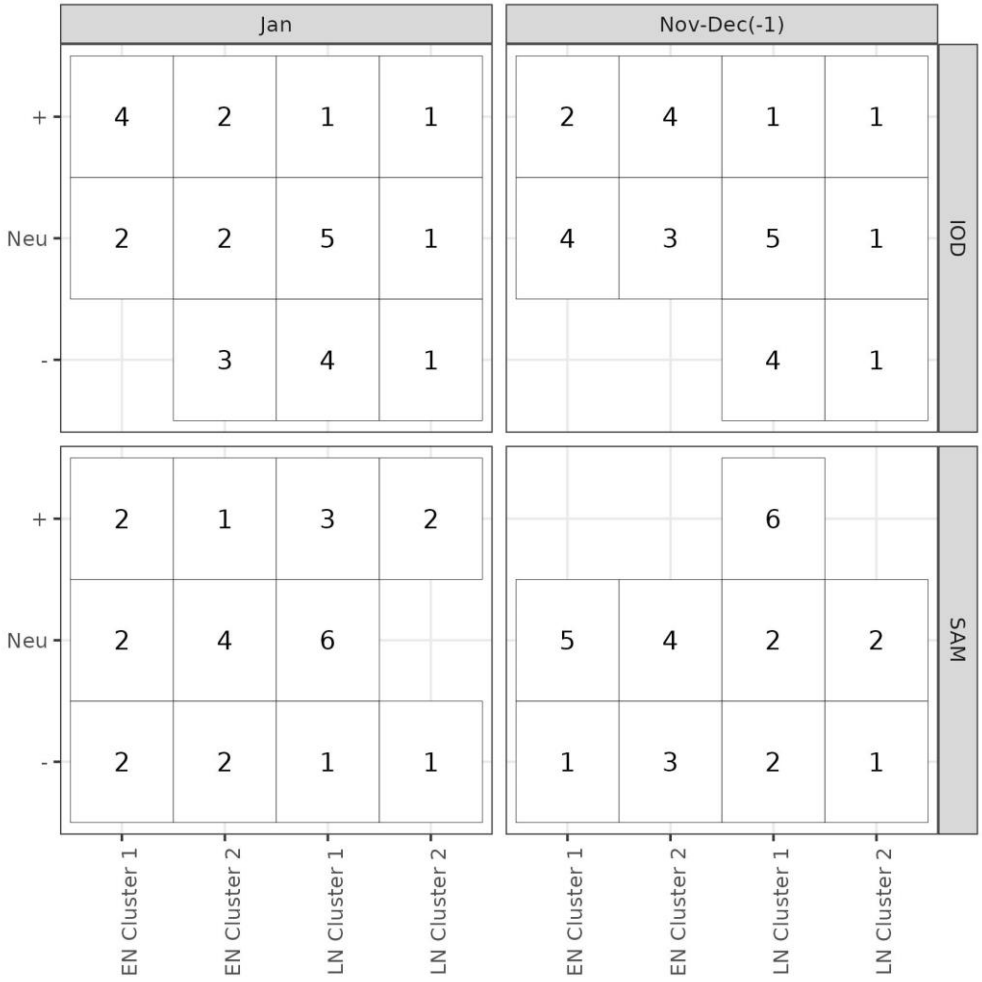

Figure 6. Contingency tables of ENSO Clusters and climate indices. The x-axis refers to the ENSO events (EN and LN) and the defined Clusters. The y-axis refers to the index value category. Numbers refer to the amount of cases that simultaneously occur the events matching the x-axis and the y-axis. The upper panels stand for IOD and the lower panels for SAM. The left panels are for the climate indices in January, and the right panels are for the climate indices in the previous months (Nov-Dec).

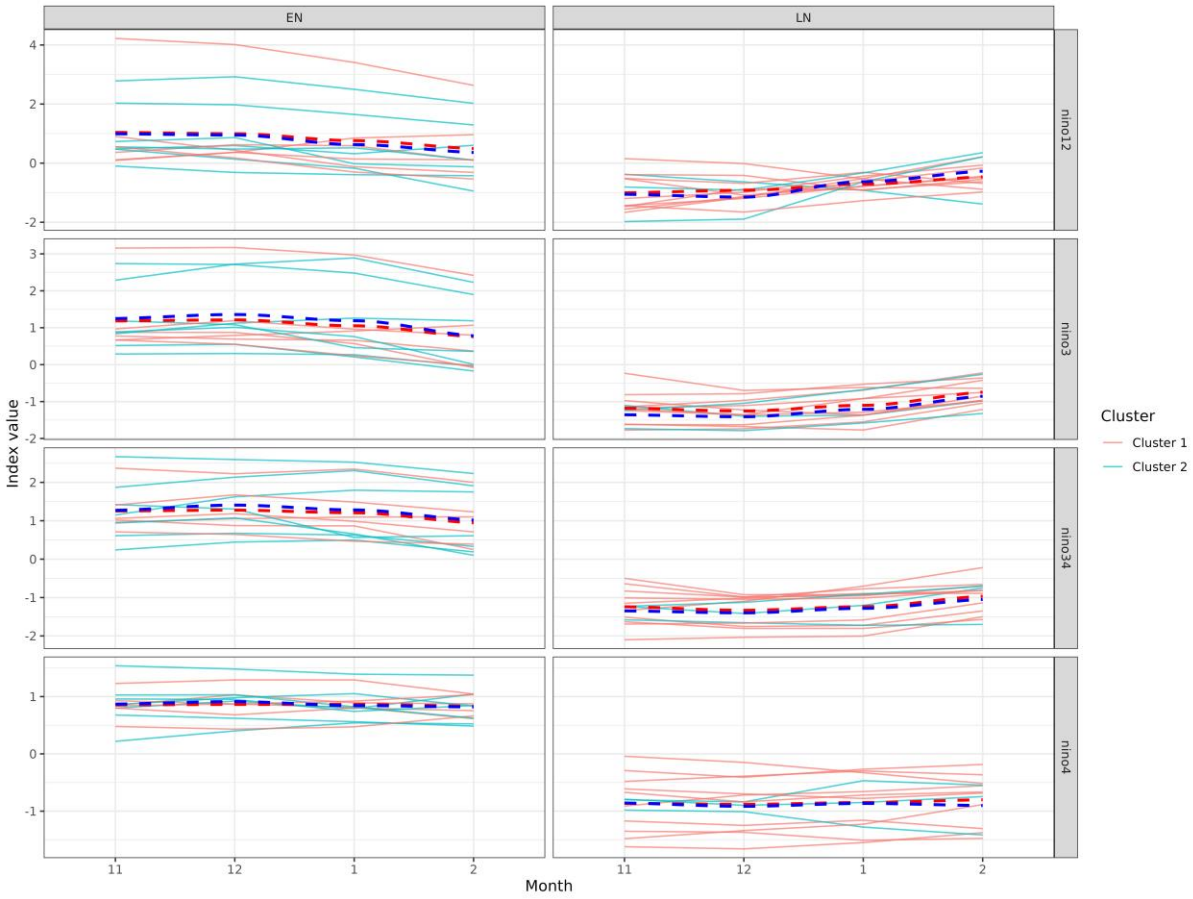

Figure 7. ENSO indices values from November (month 11) to February (month 2). Colors refer to each Cluster. The stroked lines show the monthly mean value for each cluster. The left panels show the EN events and the right panels the LN events. Each row panel shows a different ENSO index.

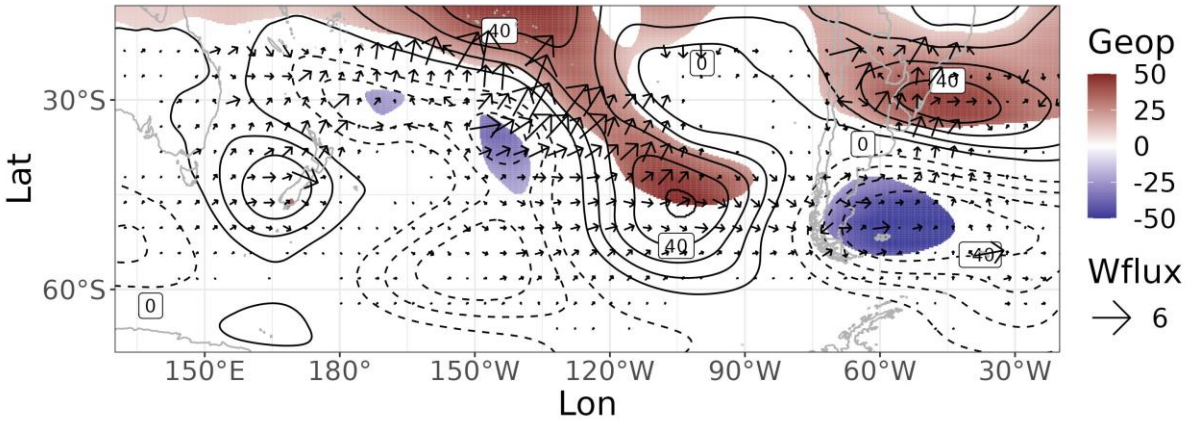

562

Figure S1. January GH (contours and color) and Wflux (arrows) composite anomalies at 250
564 hPa for the EN events in cluster 1 group. Color shades stand for significant anomalies at a 90% confidence level. Dashed contours stand for negative anomalies. The baseline period for the
566 anomalies is 1980-2010.

568

570